



Synthesis, characterization, and adsorption capacity of sodium alginate poly grafted (fumaric acid-co-polyacrylic acid)/graphene oxide hydrogel as adsorbent for Cr (VI) and Pb (II) removal

Hiba Alnasery¹ · Abdolhossein Naseri¹ · Layth Samir Jasim² · Sanaz Sajedi-Amin¹

Received: 2 December 2023 / Accepted: 30 April 2024 / Published online: 18 May 2024
© Iranian Chemical Society 2024

Abstract

This study involves the preparation of sodium alginate poly grafted (fumaric acid-polyacrylic acid)/graphene oxide, SA-g-p(FA-AA)/GO hydrogel to explore its potential as a promising adsorbent for water treatment mainly chromium (VI) and lead (II) removal. Prepared adsorbent was characterized by FTIR, TGA, XRD, FESEM, and TEM techniques for exploring the chemical structure, thermal stability, crystallography, surface area and morphology, as well as pore size and distribution of SA-g-p(FA-AA)/GO, respectively. The average size of the prepared nanoparticles was observed to be 78.48 nm. The TEM images exhibit a predominantly spherical shape and heterogeneous. Effect of different physiochemical parameters such as pH, temperature, adsorbent dosage, and contact time was explored for maximum metal adsorption. The results of the study revealed that the maximum adsorption capacity of SA-g-p(FA-AA)/GO (0.045 mg g^{-1} for Cr (VI) and 22.371 mg g^{-1} for Pb (II)) was achieved under optimized conditions, i.e., adsorbent dose of 0.05 g at 25 °C for pH of 2, 4.5 when contact time of 5 and 100 min was used for Cr(VI) and Pb(II), respectively. Data fits best to the pseudo-second-order kinetic equation revealing the multilayer adsorption of Cr (VI) and Pb (II) ions on the heterogeneous adsorbent surface. Thermodynamically, the process of Cr (VI) and Pb (II) adsorption was non-spontaneous, exothermic and feasible revealing the potential of the prepared adsorbent to be used as an efficient adsorbent for metal removal.

Keywords Sodium alginate-based hydrogel · Adsorption · Heavy metals · Nanocomposite

Introduction

In today's society, water is one of the key necessities for survival of all types of organisms. However, water resources are getting polluted every day due to different types of pollutants that leads to shortage of fresh and clean drinking water as almost 1/3rd of the total world inhabitants are facing the problems of clean water shortage. Industrial effluents are the leading source of chemical pollutants that contains a mixture of mineral anions, dyes, heavy metals, and pathogenic substances. These pollutants when enter to the

environment without any proper treatment, they result in deteriorating the water quality thus posing a serious threat to ecosystems, human health, and the overall balance of the environment. Wastewater treatment has the potential to offer alternative options for the current water supply thereby leading to enhanced water security [1–3]. Among various water pollutants, heavy metals such as lead, and chromium can cause serious negative impacts on the environment and human health [4]. These metals are non-biodegradable, which can persist in the environment for a prolonged time thus leading to bioaccumulation and biomagnification. The World Health Organization (WHO) and the European Union (EU) have established a permissible limit for total lead and chromium in drinking water that comes to be $< 0.01 \text{ ppm}$ and 0.02 ppm , respectively [5, 6]. To mitigate the problems caused by metal loaded water, it is crucial to develop some effective monitoring and removal strategies for these heavy metals from water sources.

Wide variety of techniques available for heavy metal wastewater treatment include physical treatment (filtration,

✉ Abdolhossein Naseri
a_naseri@tabrizu.ac.ir

✉ Layth Samir Jasim
layth.alhayder@qu.edu.iq

¹ Department of Analytical Chemistry, Faculty of Chemistry, University of Tabriz, P.O. Box 51644 -14766, Tabriz, Iran

² University of Al- Qadisiyah, Al- Qadisiyah, Iraq

sedimentation, and flotation), chemical treatment (coagulation, flocculation, and oxidation), electrochemical treatment, biological treatment, membrane-based methods and adsorption [7–9]. Among these methods, biological treatment and adsorption have garnered significant attention and widespread application in research endeavors due to their eco-friendly, cost-effective, energy-efficient, highly efficient, adaptable nature and addressing growing concerns over heavy metal pollution [10].

The adsorption method stands out as an intriguing process for wastewater treatment compared to conventional methods because of its remarkable attributes such as a high adsorption capacity, rapid adsorption kinetics, and the ability to selectively trap target analytes [11, 12].

Hydrogels are soft materials that consist of three-dimensional networks of hydrophilic polymers. They possess the capacity to absorb high amount of water and promote rapid transport of substance throughout their internal structure. In recent years, there has been an increasing focus on the use of hydrogels as superabsorbent [13–15]. The synthesized hydrogel-based superabsorbent using biological substrates such as sodium alginate, chitosan, cellulose and lignin can effectively remove many pollutants from aqueous solutions [16–18]. Sodium alginate (SA) is a natural polysaccharide derived from brown algae, carries a negative charge due to the presence of carboxyl functionalities on its surface. SA-derived adsorbents have gained researcher's attention due to their remarkable ability to adsorb substances, as well as their high levels of biocompatibility and biodegradability [19, 20]. However, their efficiencies can further be improved by the addition of some crosslinker agents or chemical modifications. Generally, adsorption methods utilize SA-carbon composites and SA-polymer composites due to their high surface areas, excellent stability, robust mechanical strength, and presence of numerous surface functional groups that aid in adsorption [21]. Graphene oxide, as a carbon atom lattice structure possesses oxygen functional groups, such as hydroxyl (–OH), epoxy (–O–), and carboxyl (–COOH) groups. SA has been broadly investigated with GO and results provide excellent heavy metal adsorption process due to the high mechanical strength and surface area [21, 22].

Cross-linking is the process of creating an alginate three-dimensional framework with incorporating additional characteristics into it [23, 24]. Cross-linkers play two roles (*i*) they can be directly attached to the alginate structure, or (*ii*) they can act as mediators to link different polymers with the alginate skeleton. Some common cross-linkers used in the synthesis of SA-based adsorbents include epichlorohydrin, calcium chloride, sodium tripolyphosphate, ferric chloride, glutaraldehyde, etc. In this regard, various crosslinked CS/SA hydrogels developed for removal of heavy metals specially Cr (VI), Cu (II), Cd (II), and Pb (II). In addition to cross-linkers, graft copolymerization of alginates is another approach to modify the properties of alginate-based

materials [25, 26]. Fumaric acid (FA) and acrylic acid (AA) are two examples of monomers that can be used for grafting purposes due to the presence of carboxylic acid groups, which can undergo free radical polymerization to form a graft copolymer with alginate. Furthermore, the presence of these carboxylic acid functional groups may affect the pH-responsive behavior of the resulting FA/AA grafted sodium alginate material.

Within the framework resented, this study is devoted to the synthesis and characterization of a superadsorbent SA-g-p(FA-AA)/GO composite. In this method, 3D modified SA-based composite with large surface area and high stability was prepared to adsorb heavy metal ions, namely Cr (VI) and Pb (II) from aqueous solution. To evaluate the performance of alginate-grafted copolymer composites on adsorption processes, different experimental conditions, such as adsorption dosage, contact time, pH, metal concentration, and temperature, were studied. The swelling behaviors of the superadsorbent was also investigated.

Materials and methods

Materials

Sodium alginate (SA), fumaric acid (FA), acrylic acid (AA), graphene oxide (GO), N, N'-methylene bis-acrylamide (MBA), potassium persulfate (KSP), 37% HCl, NaOH, and ethanol were procured from B.D.H company and used directly without any further modification. FeCl₃·6H₂O, NaCl, K₂S₂O₈ (KSP), NaNO₃, Pb(NO₃)₂, K₂Cr₂O₇ were supplied from Merck. All solutions were prepared using deionized water.

Synthesis of superimpose sodium alginate grafted poly (fumaric acid-acrylic acid)/ graphene oxide (SA-g-p(FA-AA) /GO)

The superimpose (SA-g-p(FA-AA)/GO) was prepared in a series of solutions, starting with dissolving 0.5 g sodium alginate in a 5 mL of distilled water and stirring with a hotplate stirrer for 60 min (solution A). Afterwards, 1 g ferric chloride, as inorganic crosslinker was dissolved in 5 mL of distilled water, and 5 g of AA monomer was added (solution B). Then, 0.05 g KSP and MBA were dissolved in 2 mL of distilled water, separately (solutions C and D). This was followed by preparing, graphene oxide solution is prepared by dissolving 0.08 g GO in 10 mL of distilled water (solution E). After that, solutions were mixed by adding solution A to solution B solution with continuous stirring for 30 min. Then, 1 g in 5 mL of FA was added and mixed for 10 min, followed by adding solution D and mixing well for 5 min. Next, solution E was added as batches and mixed

for 10 min while using N_2 for 2 min. Then, solution C was added as batches and mixed for 10 min while using N_2 for 1 min. After that, it was added in special tubes for 2 h or less in a water bath according to polymer freezing, followed by cutting and drying the composite polymer in $70\text{ }^\circ\text{C}$, cutting well, that then can be used.

Preparation and processing of the synthesized adsorbent

The preparation and processing steps employed to transform the nanocomposite hydrogel composite into a suitable adsorbent. For this, initially, the composite was carefully cut into small pieces using a sharp instrument, ensuring the creation of an optimized adsorbent surface. Subsequently, the cut pieces were thoroughly washed with ion-free distilled water while employing continuous stirring on a hot plate stirrer for a period of 1 h. Following this, the composite was separated from the water, and this washing step was repeated to eliminate any non-reactive composites.

In the next step, the composite was subjected to a drying process at $50\text{ }^\circ\text{C}$ for an entire day. This extended drying period ensures complete removal of moisture from the material. Once dried, the nanocomposite hydrogel composite was finely ground into tiny granules, yielding a powder with varying granule sizes. To achieve uniformity, appropriate sieves with different mesh sizes (ranging from 100 to $400\text{ }\mu\text{m}$) were utilized to separate the granules. The fine granules obtained through this process were utilized in the present study as the adsorbent material. Figure 1 visually represents the nanocomposite hydrogel composite after undergoing cutting, washing, drying, and grinding stages, highlighting the transformation of the material into its final state.

Characterization

The morphological characteristics of the composite materials can be analyzed using Field-Emission Scanning Electron Microscopy (FESEM) with a high-resolution (S-4800 instrument from Hitachi, Japan). In order to determine the particle size, the internal structure and atomic arrangement, Transmission Electron Microscopy (Leo, 912AB, Germany) was used. To examine the functional groups present on the surface of the studied materials, Fourier Transform Infrared Spectroscopy (FT-IR) was performed using a FT-IR instrument (Shimadzu, 8400S, Japan) with KBr tablets as sample holders in the $400\text{--}4000\text{ cm}^{-1}$ region. The crystallography of the composites can be investigated by conducting X-ray diffraction (XRD) analysis (Bruker D8 instrument from Germany), and the XRD data were collected at a scanning rate of 0.03 s^{-1} for 2θ in a range from 5° to 80° .



Fig. 1 Highlighting the transformation of SA-g-p(FA-AA)/GO into its final state as adsorbent after undergoing cutting, washing, drying, and grinding stages

Measurement of swelling ratios

For the measurement of the swelling ratios, a 0.5 g sample of the synthesized adsorbent was taken and treated in aqueous solutions with different pH values of 1.0 to 12.0. After intervals of 15 min, the adsorbent was placed on a filter paper to remove the excess solution. Subsequently, the weight of the compound was noted. The swelling ratios (S , g g^{-1}) were calculated using Eq. (1):

$$S = \frac{W_s - W_d}{W_d} \times 100 \quad (1)$$

where W_s and W_d refers to the weight of the swollen and dried sample, respectively.

Adsorption studies

The adsorption of heavy metals (Cr (VI) and Pb (II)) using SA-g-p(FA-AA)/GO composite was investigated. The study examined the effect of different factors, such as initial metal concentration, pH level, contact time, and temperature on the adsorption process. The experiments were performed in 10 mL of individual water solution of each metal (Cr (VI) and Pb (II)) using 100 mg L^{-1} at $\text{pH} = 2$ containing 0.05 g of the adsorbent with continuous shaking with the speed of 150 rpm at $25\text{ }^\circ\text{C}$ for 100 min. By centrifugation, the samples were separated at a speed

of 6000 rpm for 10 min. Afterwards, the residual concentration of ions in the solution were determined by a flame atomic absorption spectrometry (FAAS, AA-7000, Shimadzu, Japan). The adsorption capacity of adsorbent for each metal (q_e , mg g^{-1}) and removal efficiency, % RE, were calculated according to Eq. (2) and (3), respectively:

$$q_e = \frac{C_0 - C_e}{m} \times V \quad (2)$$

$$\%RE = \frac{C_0 - C_e}{C_0} \times 100 \quad (3)$$

While C_0 and C_e are the initial concentration and equilibrium concentration of metal (mg L^{-1}), respectively. Also, V is the volume of aqueous solution (L) and m is the amount of adsorbent (g).

Results and discussion

Figure 2 shows the schematic steps for the synthesis a SA-g-p(FA-AA)/GO composite. The synthesis method generally consists of two steps. I) free radical polymerization, II) covalent functionalization. In first step, the SA chemically cross-linked with AA and FA (comonomers), MBA (organic cross-linker), FeCl_3 (inorganic cross-linker), and KSP (initiator) resulting in the formation of a get gel-like solution. In the second step, the obtaining 3D modified sodium alginate (SA-g-p(FA-AA)) hydrogel was immersed in GO solution to yield chemically cross-linked network was formed due to the hydrogen bond via GO and SA.

Characterization of SA-g-p(FA-AA)/GO

FTIR of the nanocomposite hydrogel is shown in Fig. 3. FTIR characterization of SA-g-p(FA-AA)/GO showed

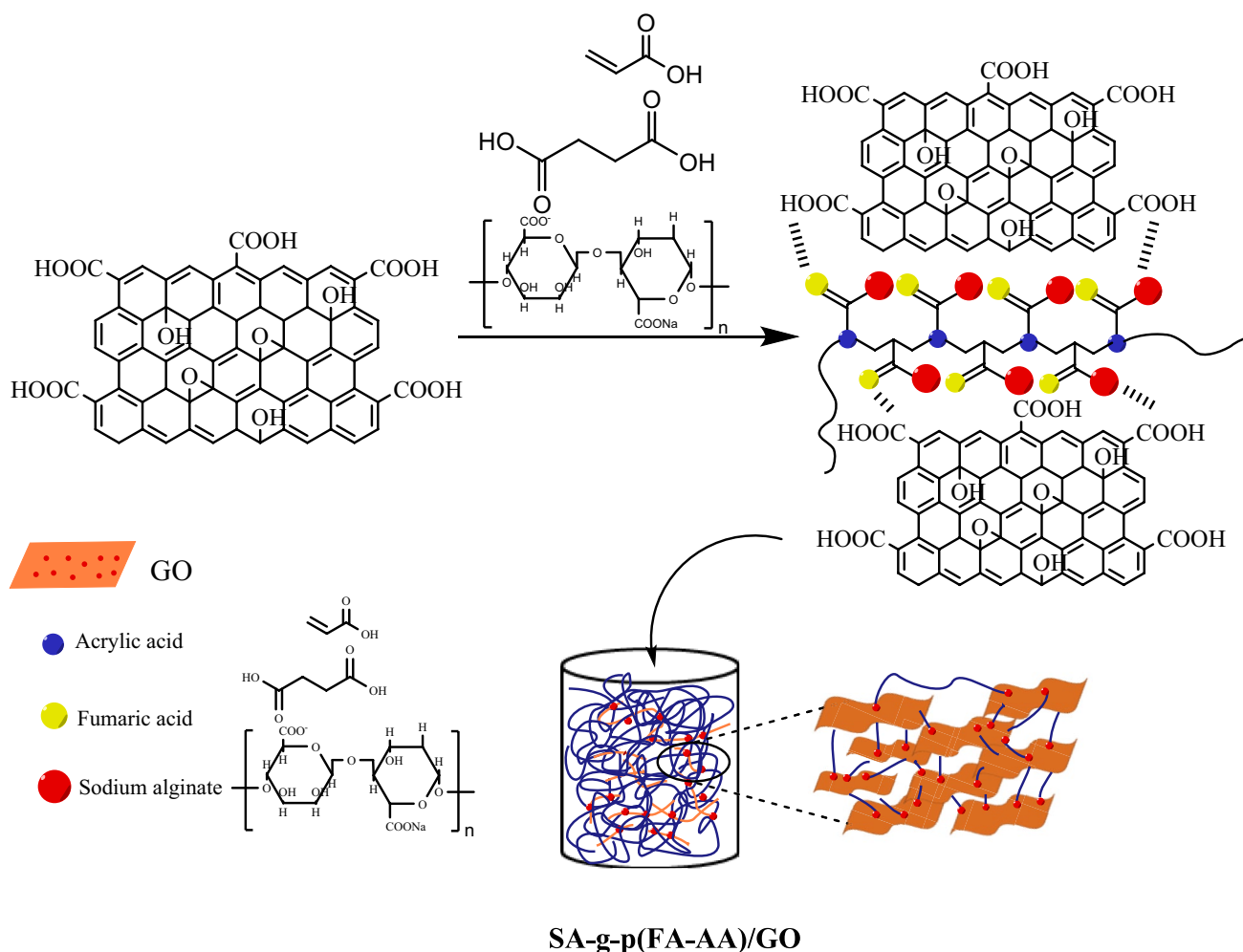


Fig. 2 The schematic illustration of the steps for the synthesis a SA-g-p(FA-AA)/GO composite

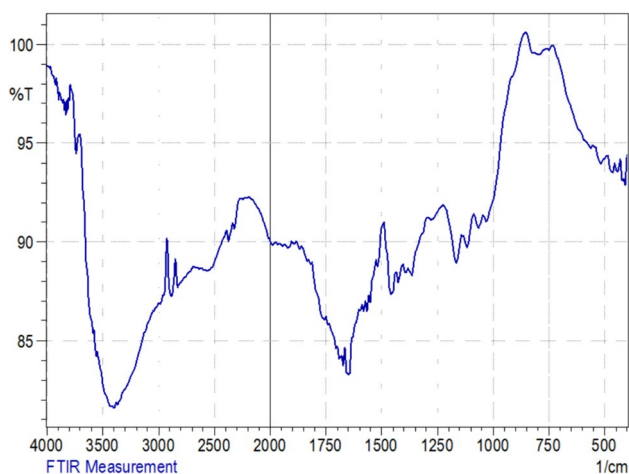


Fig. 3 FTIR of the nanocomposite hydrogel for SA-g-p(FA-AA)/GO

broadband area at the $3548\text{--}3209\text{ cm}^{-1}$ range, indicating interference between O–H in the carboxyl and hydroxyl groups, N–H in the cross-linker Methylene bis-acrylamide (MBA), and a band at 2985 cm^{-1} corresponds to the symmetrical and asymmetric stretching vibrations of --CH_2 groups of the aliphatic composites in the nanocomposite hydrogel. Moreover, the band at 1720 cm^{-1} corresponds to the carbonyl group C=O in the carboxyl acid. The bands ($1543\text{--}1410\text{ cm}^{-1}$) represented symmetrical and asymmetric vibrations of both --COO groups due to sodium alginate (SA). Further, the bands in the range $1396\text{--}1010\text{ cm}^{-1}$ were due to the O–H, N–H, and C–H groups. There were no bands for (Na–O), thus conforming to the interference of the acrylic acid (AA) and sodium alginate (SA).

The XRD spectra of the hydrogel [SA-g-p(FA-AA)] and the composite [SA-g-p(FA-AA)/GO] (Fig. 4) indicated

broadband in the angle range $2\theta = 15\text{--}30^\circ$ for the hydrogel and in the range $2\theta = 17\text{--}43^\circ$ for the composite, indicating the non-crystal nature of the hydrogel and the composite structure. XRD spectrum of the hydrogel revealed an acute and high band in the range $2\theta = 20.339^\circ$ within the calculated interlayer distance ($d = 4.3627\text{ \AA}$). Regarding the composite, there was a broad and low band at an angle of $2\theta = 21.192^\circ$ within the calculated interlayer distance ($d = 4.1891\text{ \AA}$). The comparison of XRD spectra between GO and the composite revealed that the band at $2\theta = 11.60^\circ$ was no longer present in the composite spectrum. This observation suggests that the multilayer structure of GO underwent exfoliation, dispersion, and spreading, resulting in the formation of individual layers within the three-dimensional network of the polymer composite [GO/poly(AAC-MCC)] [27].

For better understanding of the surface charge, point of zero charges (pH_{pzc}) play a major role particularly in the adsorption behavior of synthesized nanoparticles and nanocomposites. pH_{pzc} is the pH at which a nanoparticle's or nanocomposites' surface charge is zero. The pH drift technique was used to compute SA-g-p(FA-AA)/GO's pH_{pzc} (Fig. 5) and it was found to be 4.2 for SA-g-p(FA-AA)/GO. The nanocomposite attains positive surface charge at pH lower than 4.2. This positively charged surface leads to electrostatic interaction with the negatively charged analyte. As the pH increases, more of this functional group become deprotonated and resulting in its affinity to cations.

To analyze the surface morphology (porous or smooth) of the nanocomposite hydrogel, size and form of granules, nature of distribution on the surface, and bonding of polymer series, field emission-scanning electron microscopy (FESEM) was utilized. Results of the study revealed that GO was added to the hydrogel to improve its surface roughness, which is very useful for target analyte's adsorption,

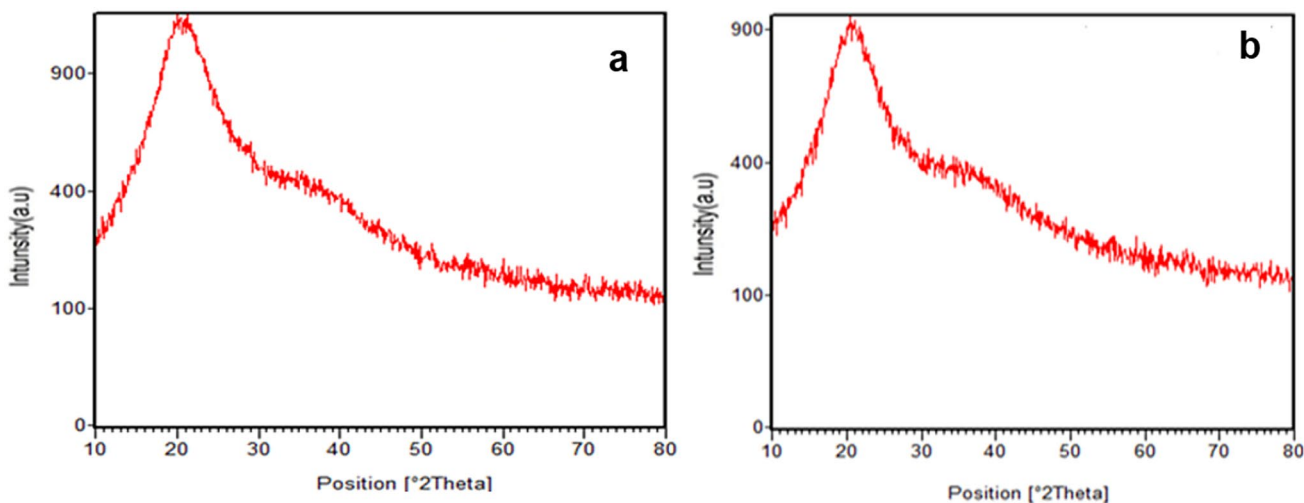


Fig. 4 XRD spectra of: **a** SA-g-p(FA-AA) and **b** SA-g-p(FA-AA)/GO

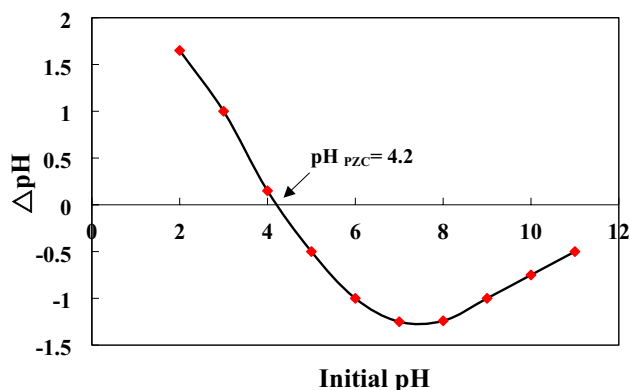


Fig. 5 The zeta potential of SA-g-p(FA-AA)/GO

enabling seeing the nanocomposite's internal pores during formation Fig. 6a. Furthermore, as shown in the figure, the average dimensions of nanoparticles in SA-g-p(FA-AA)/GO were < 78.48 nm.

To provide detailed information about the internal structure of SA-g-p(FA-AA)/GO composite, TEM analysis was used (Fig. 6b). The results of the study revealed that the SA-g-p(FA-AA)/GO particles exhibit a predominantly spherical and heterogeneous shape.

Swelling studies

The swelling behavior of SA-g-p(FA-AA)/GO composite were investigated by immersing the same amount of each

hydrogel in water and measuring their swelling ratios at different pH levels. It was observed that the swelling ratio is greatly influenced by the acidic function. Results of the study have been summarized in Fig. 7 revealing that the swelling ratio increases with the rise in acidic function. Specifically, at pH = 7, a higher swelling ratio was noted in comparison to pH = 1. This phenomenon can be attributed to the chemical composition of the maize composite, which contains hydrophilic groups (COOH, OH, C=O). These groups ionize at an acidic function of pH = 7, transforming into negative groups, leading to electrostatic repulsion among them. Consequently, this repulsion causes the polymer chains in the chemical composition to separate from each other, facilitating the ingress of water molecules and

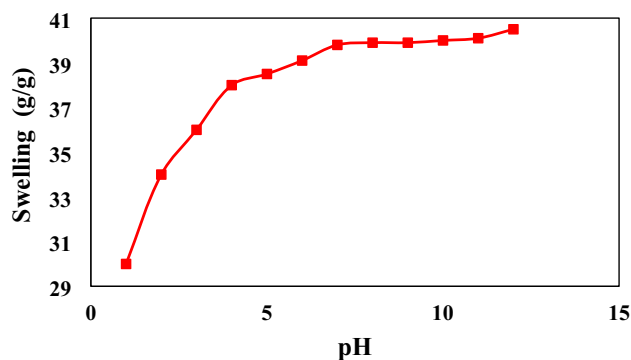


Fig. 7 The swelling behavior of SA-g-p(FA-AA)/GO hydrogel at different pH levels

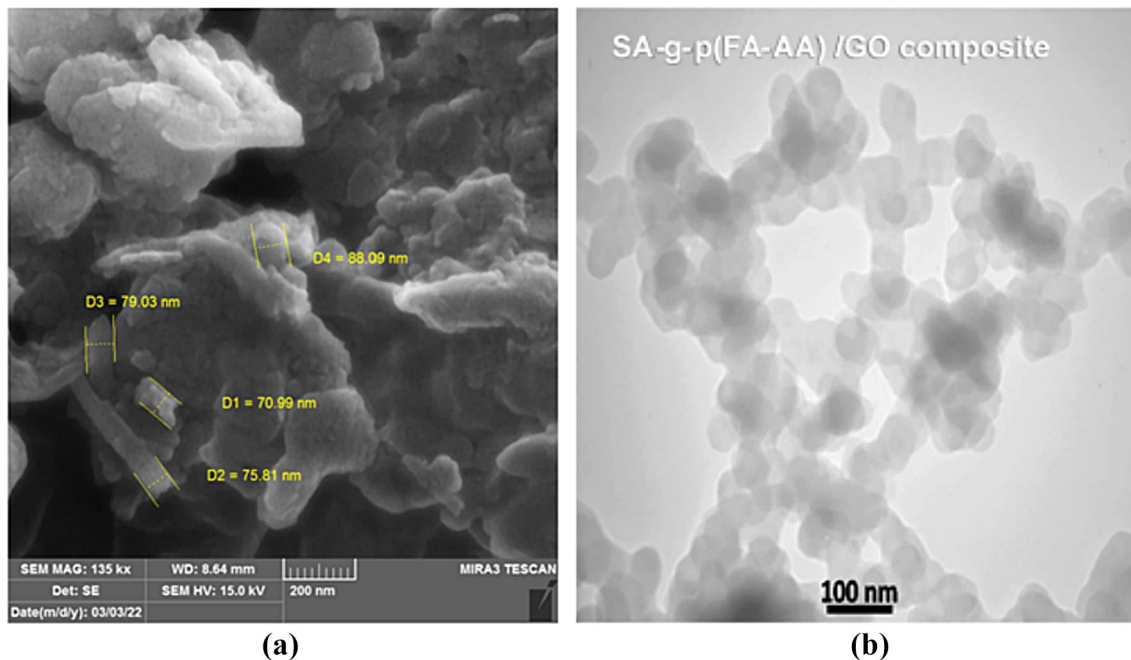


Fig. 6 **a** FESEM of SA-g-p(FA-AA)/GO composite and **b** TEM of SA-g-p(FA-AA)/GO composite

resulting in swelling. This process results in increasing the swelling ratio. Conversely, at a pH value of 1, the swelling ratio is observed to be lower. This is because of the reason that the functional groups become protonated, leading to the development of the hydrogen bonding with each other. As a result, electrostatic attraction occurs between the groups, which leads to a decrease in the swelling ratio.

Adsorption process

The ability of adsorbent material to remove Cr (VI) and Pb (II) from aqueous solutions was due to the presence of diverse functionalities in the prepared adsorbent. By chemically modifying SA with substances like GO, AA and FA, the number of binding sites can be increased, consequently improving its binding ability. In SA-g-p(FA-AA)/GO composites, the negatively charged carboxylate groups present in the sodium alginate chain interact with the positively charged cationic metals through electrostatic forces, while the oxygen-containing functional groups of graphene oxide provide additional adsorption sites for the adsorption of the heavy metals. The porous structure of graphene oxide also allows the diffusion of the metals into the composite structure, enhancing their % removal.

The adsorption of metal ions onto an adsorbent's surface is significantly affected by the pH of the solution, due to its impact on both the adsorbent's surface charge and the different forms of the metal ions. Figure 8a reveals the removal efficiency of Cr (VI). It was observed that the predominant form of hexavalent chromium, changes with the change in solution pH. Cr (VI) commonly exists in solution as an anion $\text{Cr}_2\text{O}_7^{2-}$, CrO_4^{2-} and HCrO_4^- . As per the results, it can be inferred that the highest removal efficiency for Cr (VI) would be observed at a $\text{pH} < \text{pH}_{\text{pzc}}$, where the adsorbent surface carries a positive charge. The oxygen-containing functional groups on the adsorbent surface can also coordinate with the Cr (VI) ions via hydrogen bonding and chemical complexation. Furthermore, the effect of pH on Pb (II) removal was also examined within the range of 2–9. Figure 8a shows that the % removal of Pb (II) decreases gradually with an increase in solution pH. This trend can be attributed to the solubility and speciation of the Pb (II) ions in solution. Therefore, the removal efficiency of proposed composite need to be optimized by adjusting the pH of the surrounding solution at 2–3, 4.5 for Cr (VI) and Pb (II), respectively.

In addition to solution pH, dose of the adsorbent is also an important factor affecting the adsorption processes in terms of the adsorption capacity, efficiency, and the time required to reach equilibrium. To ensure the maximum adsorption capacity, the effect of the adsorbent dose on the removal of Cr (VI), and Pb (II) in the range of 0.01–0.06 g was investigated. Results of the study revealed that as the

weight of the adsorbent (W_t) increases to 0.04 g, no obvious change was observed for Pb (II) adsorption. However, with further increase in adsorbent dose, % adsorption increases allowing for equilibrium between the adsorbate and the adsorbent to occupy all the available active sites on the adsorbent surface. This results in an increase in % adsorption on the surface, with the maximum adsorption capacity or saturation achieved when all active sites are filled by the adsorbate. However, by further increase in adsorbent dose, no significant increase in the removal efficiency of Pb (II) was observed.

The effect of contact time for Pb (II) and Cr (VI) adsorption on the SA-g-p(FA-AA)/GO nanocomposite hydrogel was investigated to determine the required equilibrium time and the results are shown in Fig. 8b. The contact time was varied from 1 to 180 min at constant experimental conditions of 25 °C, $\text{pH} = 2.5$ and 4.5, a fixed weight of 0.06 g, and a concentration of 100 ppm for each metal. Based on the study's findings, the required equilibrium time was determined to be 5 and 100 min for removal of Pb (II) and Cr (VI), respectively. It was observed that Cr (VI) reached its maximum efficiency quickly and remained constant with further increase in time. Within the first 5 min, the removal efficiency was evident, i.e., it increases from 0 to 43%, and thereafter, slight changes were recorded until the maximum removal efficiency of 48% was achieved after 180 min. In case of the adsorption of the Pb (II), results revealed that the adsorption rate was slower in the beginning which then gradually increases with time until it reached a constant maximum removal efficiency after 100 min. The difference in adsorption behavior between the two metal ions could be attributed to their different physical and chemical properties, such as size, charge density, and electronic configuration. Cr (VI) is a smaller ion with a higher charge density, which allows it to develop stronger electrostatic interactions with the adsorbent surface and thus adsorb more quickly. Pb (II), on the other hand, is a larger ion with a lower charge density and thus has weaker interactions with the adsorbent surface, leading to slower adsorption kinetics. Generally, the initial quick increase in adsorption of metal ions were due to the availability of the numerous active sites present on the adsorbent surface. As the metal ions occupied the active sites, the adsorption process became slower and more challenging as evident from kinetic study.

Wastewater can contain various types of salts in addition to metal ions. The presence of salt in the adsorption process can affect the selectivity and efficiency of the adsorption process. Chloride and carbonate are the most frequently occurring anions in wastewater samples. Hence, an experiment was also conducted to examine the influence of different salts including NaCl, KCl, and CaCO_3 on the removal of the studied metal by adsorption, Fig. 8c, d. Under the optimal experimental conditions, a suitable

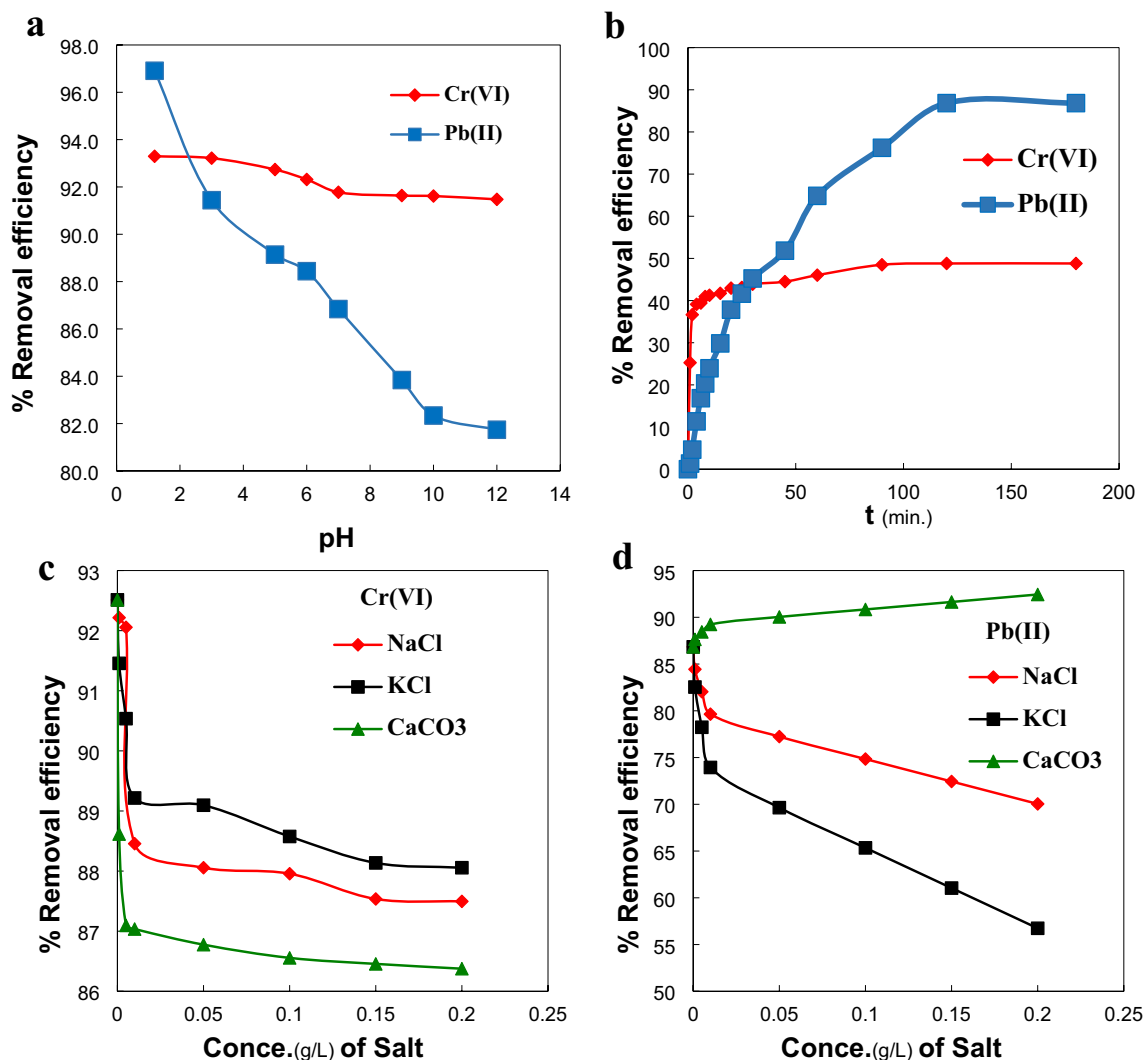


Fig. 8 **a** Effect of pH on the adsorption capacity of Cr (VI) and Pb (II) on the SA-g-p(FA-AA)/GO nanocomposite hydrogel ($C_0=50$ and $10 \text{ mL } (100 \text{ mg L}^{-1})$ for Cr (VI) and Pb (II), temperature= 25°C , stirring rate 700 rpm and $W_t=0.05 \text{ g}$), **b** Effect of contact time on Cr (VI) adsorption ($C_0=50 \text{ mL } (100 \text{ mg L}^{-1})$, temperature= 25°C , stirring rate 700 rpm and $W_t=0.05 \text{ g}$), **c** Salt effect on Cr (VI) adsorption ($C_0=50 \text{ mL } (100 \text{ mg L}^{-1})$, temperature= 25°C , stirring rate 700 rpm and $\text{pH}=2$, $W_t=0.05 \text{ g}$), **d** Salt effect on Pb (II) adsorption ($C_0=50 \text{ mL } (100 \text{ mg L}^{-1})$, temperature= 25°C , stirring rate 700 rpm and $\text{pH}=4.5$, $W_t=0.05 \text{ g}$)

amount of each salt in concentration range of $0.001\text{--}0.2 \text{ g L}^{-1}$ was introduced into each metal solution that had an initial concentration of 1000 mg L^{-1} at an optimum pH. Results of the study showed that for both of studied metals, the removal efficiency was reduced as the concentration of salts were increased. The % removal of the Cr (VI) was more efficiently affected by CaCO_3 that results in a decrease in the removal efficiency from 92.5% to about 87.5% while on the other hand, NaCl demonstrates a lower level of effect on the removal efficiency of the adsorbent. Furthermore, KCl displays the least efficient performance amongst the three tested ions. These results can be attributed to their ability to compete with the adsorbate for the adsorption sites, resulting in reduced adsorption efficiency.

and $\text{pH}=2$ and 4.5 , $W_t=0.05 \text{ g}$ for Cr (VI) and Pb (II)), **c** Salt effect on Cr (VI) adsorption ($C_0=50 \text{ mL } (100 \text{ mg L}^{-1})$, temperature= 25°C , stirring rate 700 rpm and $\text{pH}=2$, $W_t=0.05 \text{ g}$), **d** Salt effect on Pb (II) adsorption ($C_0=50 \text{ mL } (100 \text{ mg L}^{-1})$, temperature= 25°C , stirring rate 700 rpm and $\text{pH}=4.5$, $W_t=0.05 \text{ g}$)

Kinetic studies

The kinetic study of the adsorption process is necessary to determine the best-fit model for the adsorption process and to obtain information on the adsorption mechanism. Two commonly used models are the pseudo-first-order and pseudo-second-order kinetic models, which are expressed in Eqs. (4) and (5), respectively.

$$\ln(q_e - q_t) = \ln q_e - k_1 t \quad (4)$$

$$\frac{t}{q_t} = \frac{1}{k_2 q_e^2} + \frac{1}{q_e} t \quad (5)$$

The equations include rate constants k_1 (min^{-1}) and k_2 ($\text{g mg}^{-1} \text{min}^{-1}$) for the pseudo-first-order and pseudo-second-order adsorption models, respectively. Also, q_e and q_t are the amounts of analytes adsorbed at equilibrium and time t (mg g^{-1}). The adsorption kinetic plots and the linear fitted data are shown in Fig. 9. The kinetic parameters obtained from various kinetic models are listed in Table 1.

Based on the determination coefficients being closer to 1 for the pseudo-second-order kinetic model compared to the pseudo-first-order kinetic model, it can be inferred that the current adsorption system is predominantly following the pseudo-second-order rate model for both adsorption of Pb (II) and Cr (VI) on SA-g-p(FA-AA)/GO nanocomposite. The obtained values of k_2 from the assessment of the pseudo-second-order kinetic model represent the rate constant for adsorption of Pb (II) and Cr (VI) on SA-g-p(FA-AA)/GO nanocomposite. The value of 9.852 for Cr (VI) suggests faster adsorption when compared with Pb (II) with a value of 0.019, which is consistent with the findings depicted in Fig. 8b. The maximum adsorption capacities, as determined by the pseudo-second-order model, are $22.3714 \text{ mg g}^{-1}$ for Pb (II) and 0.0447 mg g^{-1} for Cr (VI). This indicates that the adsorption capacity for Pb (II) is higher than that of Cr (VI), suggesting that a greater number of Pb ions are absorbed

by the nanocomposite compared to Cr ions when reaching equilibrium under identical experimental conditions. This may be due to the preference of the sorbent for interacting with Pb ions over Cr ions. Table 2 lists a comparative study of adsorption capacities for the prepared SA-g-p(FA-AA)/GO nanocomposite with SA-based adsorbent in the literature for the removal of heavy metals from water.

Adsorption isotherm study

Adsorption isotherms provide valuable information about the behavior of adsorption of molecules on a solid surface, the capacity and selectivity of adsorbents, and the surface properties of the adsorbent (i.e. surface area, pore size distribution). By evaluating the equilibrium adsorption capacities, various adsorption systems and conditions can be compared. Several isotherm models, such as Langmuir, Freundlich and Temkin isotherms, were investigated on the concentration data of the study.

Langmuir's isotherm theory assumes that the surface of the adsorbent is homogeneous, and uniform, and that the adsorption process is reversible. According to this theory, the adsorbate molecules are assumed to adsorb onto the surface of the adsorbent until all available adsorption sites

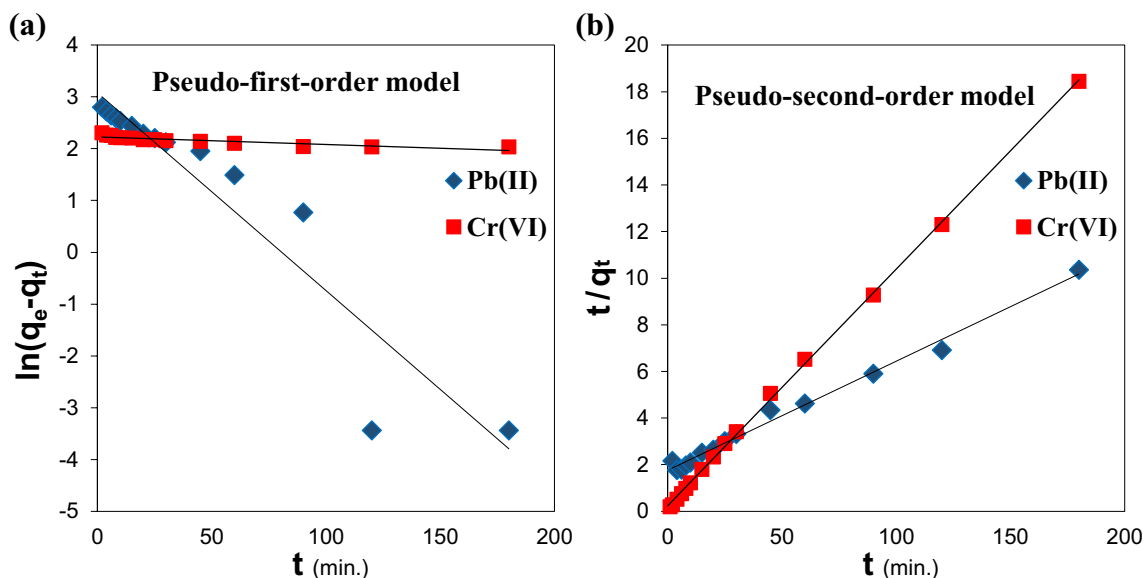


Fig. 9 a pseudo-first-order and b pseudo-second-order kinetic models for adsorption of Pb (II) and Cr (VI) on SA-g-p(FA-AA)/GO nanocomposite

Table 1 The kinetic parameters obtained from various kinetic models

| | Pseudo-first-order | | | Pseudo-second-order | | |
|---------|-----------------------------|------------------------------|-------|--|------------------------------|-------|
| | k_1 (min^{-1}) | q_e (mg g^{-1}) | R^2 | k_2 ($\text{g mg}^{-1} \text{min}^{-1}$) | q_e (mg g^{-1}) | R^2 |
| Pb (II) | 0.038 | 21.3190 | 0.897 | 0.019 | 22.3714 | 0.949 |
| Cr (VI) | 0.0018 | 9.5965 | 0.560 | 9.852 | 0.0447 | 0.999 |

Table 2 Comparison of removal of heavy metals with SA-based adsorbent in previous studies

| Adsorbent | analyte | q_{\max} (mg g ⁻¹) | References |
|--|---------|----------------------------------|------------|
| SA-polyacrylamide (PAM)/GO | Cu (II) | 68.76 | [28] |
| | Pb (II) | 240.69 | |
| NH ₂ -SA/ poly-N-isopropyl acrylamide (PNIPA) | Cu (II) | 57.20 | [29] |
| | Cd (II) | 100.50 | |
| Chitosan /SA/Ca ²⁺ | Pb (II) | 176.50 | [30] |
| | Cu (II) | 70.83 | |
| | Cd (II) | 81.25 | |
| SA-g-poly(acrylic acid-co-acrylamide) | Pb (II) | 231.88 | [31] |
| | Cd (II) | 235.62 | |
| | Ni (II) | 67.52 | |
| | Cu (II) | 76.35 | |
| SA-g-p(FA-AA)/GO | Pb (II) | 22.371 | This work |
| | Cr (VI) | 0.0447 | |

are occupied. In other words, adsorption is considered as a monolayer. The Langmuir equation can be represented as follows:

$$q_e = q_m K_L \frac{C_e}{1 + K_L C_e} \quad (6)$$

where C_e represents equilibrium concentration (mg L⁻¹), q_e the amount adsorbed at the equilibrium (mg g⁻¹). The q_m (mg g⁻¹) indicates the maximum adsorption capacity of the monolayer, and K_L (L mg⁻¹) indicates the Langmuir adsorption constant. The Langmuir's linear equation form can be expressed as below:

$$\frac{C_e}{q_e} = \frac{1}{K_L q_m} + \frac{C_e}{q_m} \quad (7)$$

The R_L parameter, also known as the separation factor is a dimensionless quantity used in the Langmuir isotherm equation. It is defined as:

$$R_L = \frac{1}{1 + K_L C_0} \quad (8)$$

The R_L parameter can be used to evaluate the favorability of the adsorption process; R_L values less than 1 indicate favorable adsorption, while R_L values greater than 1 indicate unfavorable adsorption.

Unlike the Langmuir isotherm model, the Freundlich isotherm model assumes the surface of the adsorbent as heterogeneous and suggesting the multilayer adsorption. This model can be expressed mathematically by an equation given below:

$$q_e = K_F C_e^{\left(\frac{1}{n}\right)} \quad (9)$$

Linear form of the equation is given as:

$$\log q_e = \log K_F + \frac{1}{n} \log C_e \quad (10)$$

where K_F (mg¹⁻ⁿ Lⁿ g⁻¹) shows the adsorption capacity and $\frac{1}{n}$ shows the adsorption intensity. The value of 'n' generally ranges from 0.1 to 1.0, and values greater than 1 indicate that the adsorption process is favorable, while values less than 1 denote unfavorable adsorption. A value of n equal to 1 signifies a linear relationship between q and C, suggesting that the surface of the adsorbent is homogeneous. Additionally, this variable helps in distinguishing the kind of adsorption either physical or chemical adsorption. Where n is greater than 1, the adsorption process is mainly a physical one, while if n is less than 1, the adsorption process is primarily chemical in nature.

Another isotherm model, i.e., the Temkin isotherm is another model that is useful for describing the adsorption of molecules onto materials with non-uniform adsorbent energies. In other words, this model leads to best fit when different parts of the surface have different affinities for the adsorbate molecules. The Temkin isotherm equation can be expressed as:

$$q_e = \frac{RT}{b} \ln K_T C_e \quad (11)$$

Above equation can be rearranged to a linear form:

$$q_e = \frac{RT}{b} \ln K_T + \frac{RT}{b} \ln C_e \quad (12)$$

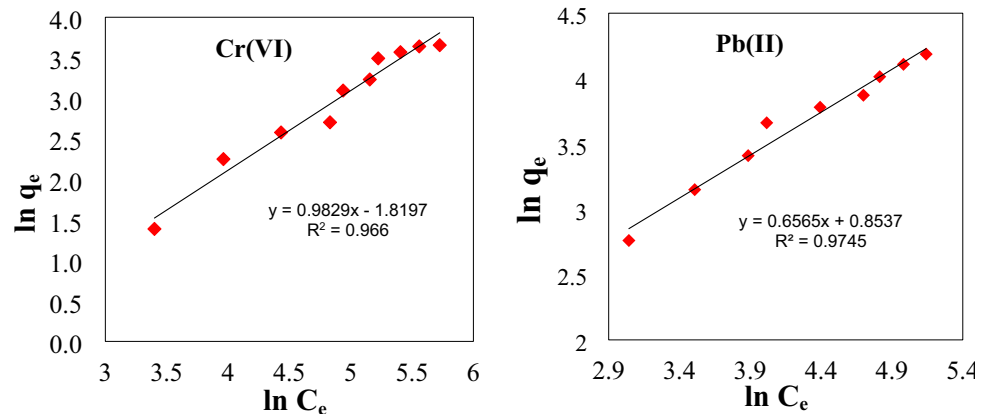
K_T is the equilibrium constant of adsorption (L mol⁻¹) and constant $B = \frac{RT}{b}$ is related to the heat of adsorption and the strength of the surface heterogeneity of the adsorbent. Also, R, T and b are the universal gas constant (8.314 J mol⁻¹ K⁻¹), the absolute temperature (K), and a constant, respectively.

Table 3 Langmuir and Freundlich and Temkin isotherm parameters and their corresponding standard errors (S.E.) along with regression coefficients (R^2) for Cr (VI) and Pb (II) adsorption on SA-g-p(FA-AA)/GO composite

| NO. | Isotherm | Model parameters | Cr (VI) | | | Pb (II) | | |
|-----|------------|------------------------------|---------|-------|-------|---------|-------|-------|
| | | | Values | S. E. | R^2 | Values | S. E. | R^2 |
| 1 | Langmuir | q_m (mg g ⁻¹) | 526.31 | High* | 0.033 | 185.18 | High* | 0.314 |
| | | K_L (L mg ⁻¹) | 0.0003 | High* | | 0.1220 | High* | |
| 2 | Freundlich | K_F (mg g ⁻¹) | 0.16 | 0.05 | 0.966 | 2.3 | 0.4 | 0.974 |
| | | n | 1.01 | 0.06 | | 1.52 | 0.09 | |
| 3 | Temkin | K_T (L mol ⁻¹) | 0.03 | 0.02 | 0.899 | 0.07 | 0.02 | 0.972 |
| | | B (J mol ⁻¹) | 16.2 | 1.9 | | 25.0 | 1.7 | |

*Not fitted to the model so the standard error of calculated model parameters is high

Fig. 10 The best fitted Freundlich isotherm for adsorption of Cr (VI) and Pb (II) on SA-g-p(FA-AA)/GO composite



All model parameters with related correlation coefficients are corroborated in Table 3 and further represented in Fig. 10.

The results reveal that current adsorption data for Cr (VI) and Pb (II) are not appropriate for Langmuir isotherm ($R^2 < 0.314$). However, Temkin isotherm showed a high correlation coefficient but the Freundlich isotherm model performs well fitting by a correlation coefficient higher than 0.966. It indicates that multilayered adsorption of metal ions takes place on the heterogeneous surface of SA-g-p(FA-AA)/GO adsorbent. In addition, n values for each metal indicate that the adsorption process is favorable and mainly physical in nature.

Thermodynamic study

Thermodynamics is a vital tool for gaining insight into the energetics of chemical reactions, phase transitions, and reaction mechanisms. To evaluate the process, thermodynamic parameters such as the changes in standard enthalpy (ΔH^0), standard entropy (ΔS^0), and standard free energy (ΔG^0) are required. Experimental data obtained at different temperatures (15, 20, 25, 30 °C) were used to calculate these parameters by Van't Hoff equation given below as:

$$K_d = \frac{q_e}{C_e} \quad (13)$$

$$\ln K_d = -\frac{\Delta G^0}{RT} = -\frac{\Delta H^0}{RT} + \frac{\Delta S^0}{R} \quad (14)$$

$$\Delta G^0 = \Delta H^0 - T\Delta S^0 \quad (15)$$

where K_d , C_e , q_e , ΔG^0 , R , T , ΔH^0 , and ΔS^0 are equilibrium constant, the equilibrium concentration of analyte (mg L⁻¹), the amount of analyte adsorbed on the adsorbent surface at equilibrium time (mg g⁻¹), change in Gibbs free energy (kJ mol⁻¹), constant of gases (8.314 J mol⁻¹ K⁻¹), the temperature in Kelvin (K), change in enthalpy (kJ mol⁻¹) and change in entropy (J mol⁻¹ K⁻¹), respectively. Table 4 presents a summary of the thermodynamic parameters obtained, including their associated uncertainties. For Cr (VI) and Pb (II), the Gibbs free energy change (ΔG^0) are positive which suggest that the reaction is non-spontaneous. This means that external energy is required for adsorption of Cr (VI) and Pb (II) on adsorbent's surface. As temperature increases, there is a corresponding increase in (ΔG^0) values, which suggests that adsorption becomes more favorable at lower temperatures.

Table 4 The thermodynamic parameters for adsorption of Cr (VI) and Pb (II) on SA-g-p(FA-AA)/GO

| | ΔG^0 (kJ mol ⁻¹) | | | | ΔH^0 (kJ mol ⁻¹) | ΔS^0 (J mol ⁻¹ K ⁻¹) |
|---------|--------------------------------------|-------------|-------------|-------------|--------------------------------------|---|
| | 288 K | 293 K | 298 K | 303 K | | |
| Cr (VI) | 3.64 ± 0.22 | 4.32 ± 0.16 | 4.85 ± 0.22 | 5.73 ± 0.16 | -34.72 ± 2.81 | -135.48 ± 9.70 |
| Pb (II) | 2.31 ± 0.16 | 2.69 ± 0.17 | 3.09 ± 0.15 | 3.14 ± 0.15 | -13.96 ± 3.28 | -57.73 ± 11.30 |

The negative values of ΔH^0 indicate that the adsorption process of studied metal was exothermic in nature. The negative sign in the entropy (ΔS^0) for adsorption indicates that the process the adsorbing species interacting with the adsorbent surface in a more ordered state of the system.

Conclusion

This paper demonstrated the synthesis of sodium alginate poly grafted (fumaric acid-polyacrylic acid)/graphene oxide (SA-g-p(FA-AA)/GO) hydrogel via combination of free radical polymerization and covalent functionalization for exploring its adsorptive potential against heavy metals. FTIR, XRD, FESEM, TEM analysis of the nanocomposite hydrogel confirmed its successful synthesis. The maximum swelling percent of SA-g-p(FA-AA)/GO composite was obtained at pH = 12. The ability of the synthesized adsorbent was examined for the removal of Cr (VI) and Pb (II). The optimized removal efficiency of the prepared composite was attained at pH = 2–3, 4.5 using 0.05, 0.06 g adsorbent amount when the contact time of 60 and 120 min was given to the adsorption of the Cr (VI) and Pb (II), respectively. The presence of salt in the adsorption process reduced the removal efficiency of the studied adsorbent. The maximum adsorption reached 0.045 mg g⁻¹ for Cr (VI) and 22.371 mg g⁻¹ for Pb (II) under the optimized conditions. It implies that more Pb ions are adsorbed on the nanocomposite compared to Cr ions under similar conditions. Langmuir, Freundlich, and Temkin isotherms were used to analyze the equilibrium data, and results revealed that the Freundlich model fits well to the experimental data revealing the multilayer adsorption of Cr (VI) and Pb (II) on SA-g-p(FA-AA)/GO. Based on kinetic study, the system is predominantly following the pseudo-second-order model for the adsorption of both Pb (II) and Cr (VI). Furthermore, the obtained rate constant values show faster Cr (VI) adsorption (having $k_2 = 9.852$) when compared to Pb (II) (having $k_2 = 0.019$). The thermodynamic parameters showed that the adsorption process was non-spontaneous and exothermic with a decrease in disorderliness at the interface between the solid and liquid phases (over a range of temperature) during the adsorption of Cr (VI) and Pb (II) on SA-g-p(FA-AA)/GO. Overall, the adsorbent prepared in this study has great potential for use as an efficient sorbent to remove heavy metal, i.e., chromium and lead from water. In the future, the practical potential of the

SA-g-p(FA-AA)/GO hydrogel in real-world scenarios, like wastewater treatment plants and industrial effluents, need to be assessed for addressing environmental contamination issues.

Acknowledgements The authors would like to acknowledge the Research Council of University of Tabriz for their help and support.

Declarations

Conflict of interest The authors declare that they have no known competing financial interests or personal relationships that could have appeared to influence the work reported in this paper.

References

1. A. Azimi, A. Azari, M. Rezakazemi, M. Ansarpour, Removal of heavy metals from industrial wastewaters: a review. *ChemBioEng Rev.* **4**, 37–59 (2017)
2. G. Palani, A. Arputhalatha, K. Kannan et al., Current trends in the application of nanomaterials for the removal of pollutants from industrial wastewater treatment—a review. *Molecules* **26**, 2799 (2021)
3. H. Souhassou, Y. Fahoul, I. El Mrabet, et al., Optimization of basic red 29 dye removal onto a natural red clay using response surface methodology. *J. Iranian Chem. Soc.*, 1–17 (2023)
4. M.B. Poudel, M. Shin, H.J. Kim, Interface engineering of MIL-88 derived MnFe-LDH and MnFe2O3 on three-dimensional carbon nanofibers for the efficient adsorption of Cr (VI), Pb (II), and As (III) ions. *Sep. Purif. Technol.* **287**, 120463 (2022)
5. S. Water and W. H. Organization, Guidelines for drinking-water quality [electronic resource]: incorporating first addendum. Vol. 1, Recommendations. (2006)
6. F. Edition, Guidelines for drinking-water quality. *WHO Chron.* **38**, 104–108 (2011)
7. S. Rajendran, T. Priya, K.S. Khoo et al., A critical review on various remediation approaches for heavy metal contaminants removal from contaminated soils. *Chemosphere* **287**, 132369 (2022)
8. P. Punia, M.K. Bharti, R. Dhar et al., Recent advances in detection and removal of heavy metals from contaminated water. *ChemBio-Eng Rev.* **9**, 351–369 (2022)
9. N.A. Qasem, R.H. Mohammed, D.U. Lawal, Removal of heavy metal ions from wastewater: A comprehensive and critical review. *Npj Clean Water* **4**, 36 (2021)
10. H.S. Ibrahim, N.S. Ammar, M. Soylak, M. Ibrahim, Removal of Cd (II) and Pb (II) from aqueous solution using dried water hyacinth as a biosorbent. *Spectrochim. Acta Part A Mol. Biomol. Spectrosc.* **96**, 413–420 (2012)
11. S. Rajendran, A. Priya, P.S. Kumar et al., A critical and recent developments on adsorption technique for removal of heavy metals from wastewater-A review. *Chemosphere* **303**, 135146 (2022)

12. A. Maftouh, O. El Fatni, S. El Hajjaji et al., Comparative review of different adsorption techniques used in heavy metals removal in water. *Biointerface Res. Appl. Chem* **13**, 397 (2023)
13. H. Zhu, S. Chen, Y. Luo, Adsorption mechanisms of hydrogels for heavy metal and organic dyes removal: A short review. *J. Agric. Food Res.* **12**, 100552 (2023)
14. Z. Darban, S. Shahabuddin, R. Gaur et al., Hydrogel-based adsorbent material for the effective removal of heavy metals from wastewater: a comprehensive review. *Gels* **8**, 263 (2022)
15. M.A. Vafaei, A. Shakeri, H. Salehi et al., Cellulose nanofiber modified poly (Acrylic Acid-Co-N-Vinyl Pyrrolidone) hydrogel as forward osmosis draw agent. *J. Polym. Environ.* **31**(10), 4369–4381 (2023)
16. X. Pei, L. Gan, Z. Tong et al., Robust cellulose-based composite adsorption membrane for heavy metal removal. *J. Hazard. Mater.* **406**, 124746 (2021)
17. P.B. Vilela, A. Dalalibera, E.C. Duminelli et al., Adsorption and removal of chromium (VI) contained in aqueous solutions using a chitosan-based hydrogel. *Environ. Sci. Pollut. Res.* **26**, 28481–28489 (2019)
18. P. Santander, B. Butter, E. Oyarce et al., Lignin-based adsorbent materials for metal ion removal from wastewater: A review. *Ind. Crops Prod.* **167**, 113510 (2021)
19. X. Gao, C. Guo, J. Hao et al., Adsorption of heavy metal ions by sodium alginate based adsorbent-a review and new perspectives. *Int. J. Biol. Macromol.* **164**, 4423–4434 (2020)
20. S. Thakur, B. Sharma, A. Verma et al., Recent progress in sodium alginate based sustainable hydrogels for environmental applications. *J. Clean. Prod.* **198**, 143–159 (2018)
21. N. Mohanty, B.N. Patra, Polypyrrole-sodium alginate nanocomposites for enhanced removal of toxic organic and metal pollutants from wastewater. *Mater. Today Commun.* **34**, 105325 (2023)
22. S. Velusamy, A. Roy, S. Sundaram, T. Kumar Mallick, A review on heavy metal ions and containing dyes removal through graphene oxide-based adsorption strategies for textile wastewater treatment. *Chem. Record* **21**, 1570–1610 (2021)
23. K.Z. Elwakeel, M.M. Ahmed, A. Akhdhar et al., Recent advances in alginate-based adsorbents for heavy metal retention from water: a review. *Desalin. Water Treat.* **272**, 50–74 (2022)
24. D. Thirumoolan, T. Siva, R. Ananthakumar, K.S.N. Nambi, Alginate-Based Superabsorbents, in *Bio-based superabsorbents: recent trends, types, applications and recycling*. ed. by S. Pradhan, S. Mohanty (Springer Nature Singapore, Singapore, 2023), pp.93–114
25. A. El Idrissi, A. El Gharrak, G. Achagri et al., Synthesis of urea-containing sodium alginate-g-poly (acrylic acid-co-acrylamide) superabsorbent-fertilizer hydrogel reinforced with carboxylated cellulose nanocrystals for efficient water and nitrogen utilization. *J. Environ. Chem. Eng.* **10**, 108282 (2022)
26. K.A. Uyanga, Y. Iamphaojeen, W.A. Daoud, Effect of zinc ion concentration on crosslinking of carboxymethyl cellulose sodium-fumaric acid composite hydrogel. *Polymer* **225**, 123788 (2021)
27. Z. Li, J. Shen, H. Ma et al., Preparation and characterization of pH-and temperature-responsive nanocomposite double network hydrogels. *Mater. Sci. Eng. C* **33**, 1951–1957 (2013)
28. H. Jiang, Y. Yang, Z. Lin et al., Preparation of a novel bio-adsorbent of sodium alginate grafted polyacrylamide/graphene oxide hydrogel for the adsorption of heavy metal ion. *Sci. Total Environ.* **744**, 140653 (2020)
29. J. Tang, J. Huang, T. Tun et al., Cu (II) and Cd (II) capture using novel thermosensitive hydrogel microspheres: adsorption behavior study and mechanism investigation. *J. Chem. Technol. Biotechnol.* **96**, 2382–2389 (2021)
30. S. Tang, J. Yang, L. Lin et al., Construction of physically crosslinked chitosan/sodium alginate/calcium ion double-network hydrogel and its application to heavy metal ions removal. *Chem. Eng. J.* **393**, 124728 (2020)
31. M. Tally, Y. Atassi, Synthesis and characterization of pH-sensitive superabsorbent hydrogels based on sodium alginate-g-poly (acrylic acid-co-acrylamide) obtained via an anionic surfactant micelle templating under microwave irradiation. *Polym. Bull.* **73**, 3183–3208 (2016)

Springer Nature or its licensor (e.g. a society or other partner) holds exclusive rights to this article under a publishing agreement with the author(s) or other rightsholder(s); author self-archiving of the accepted manuscript version of this article is solely governed by the terms of such publishing agreement and applicable law.